TÜBİTAK

**Turkish Journal of Chemistry**

**http://journals.tubitak.gov.tr/chem/**

**Research Article**

Turk J Chem
(2023) 47: 1224-1238
© TÜBİTAK
doi:10.55730/1300-0527.3607

# Reducible tungsten(VI) oxide-supported ruthenium(0) nanoparticles: highly active catalyst for hydrolytic dehydrogenation of ammonia borane

**Serdar AKBAYRAK[1], Yalçın TONBUL[2], Saim ÖZKAR[3,*]**

[1]Department of Basic Sciences, Faculty of Engineering, Necmettin Erbakan University, Konya, Turkiye
[2]Ziya Gökalp Faculty of Education, Dicle University, Diyarbakır, Turkiye
[3]Department of Chemistry, Middle East Technical University, Ankara, Turkiye

**Received:** 21.03.2023 • **Accepted/Published Online:** 28.09.2023 • **Final Version:** 31.10.2023

**Abstract:** Reducible $WO_3$ powder with a mean diameter of 100 nm is used as support to stabilize ruthenium(0) nanoparticles. Ruthenium(0) nanoparticles are obtained by $NaBH_4$ reduction of ruthenium(III) precursor on the surface of $WO_3$ support at room temperature. Ruthenium(0) nanoparticles are uniformly dispersed on the surface of tungsten(VI) oxide. The obtained $Ru^0/WO_3$ nanoparticles are found to be active catalysts in hydrolytic dehydrogenation of ammonia borane. The turnover frequency (TOF) values of the $Ru^0/WO_3$ nanocatalysts with the metal loading of 1.0%, 2.0%, and 3.0% wt. Ru are 122, 106, and 83 $min^{-1}$, respectively, in releasing hydrogen gas from the hydrolysis of ammonia borane at 25.0 °C. As the $Ru^0/WO_3$ (1.0% wt. Ru) nanocatalyst with an average particle size of 2.6 nm provides the highest activity among them, it is extensively investigated. Although the $Ru^0/WO_3$ (1.0% wt. Ru) nanocatalyst is not magnetically separable, it has extremely high reusability in the hydrolysis reaction as it preserves 100% of initial catalytic activity even after the 5th run of hydrolysis. The high activity and reusability of $Ru^0/WO_3$ (1.0% wt. Ru) nanocatalyst are attributed to the favorable metal-support interaction between the ruthenium(0) nanoparticles and the reducible tungsten(VI) oxide. The high catalytic activity and high stability of $Ru^0/WO_3$ nanoparticles increase the catalytic efficiency of precious ruthenium in hydrolytic dehydrogenation of ammonia borane.

**Key words**: Ruthenium, tungsten(vi) oxide, catalytic activity, ammonia borane, reusability, hydrolytic dehydrogenation.

## 1. Introduction

Due to depletion of energy reserves [1,2] and global warming mainly caused by the increasing atmospheric $CO_2$ concentration [3], there exists an urgent request to substitute fossil fuels for the renewable energy sources on the way towards sustainable energy future [4,5]. As a green energy carrier, hydrogen is expected to have a vital role in this transition [6-8]. Conversely, the failure of safe and efficient storage of $H_2$ gas impedes its large-scale application [9-11]. Fortunately, ammonia borane (AB, $NH_3BH_3$) appears to be one of the most promising solid hydrogen storage compounds thanks to its high hydrogen content, nontoxicity, lasting stability in liquid phase and solid state, and high water solubility [12-15]. Hydrolysis of AB has been found to be the most appropriate process for liberating $H_2$ gas (Equation 1) [16-20].

$$H_3N \cdot BH_3(aq) + 2H_2O(l) \xrightarrow{catalyst} NH_4^+(aq) + BO_2^-(aq) + 3H_2(g) \quad (1)$$

Hydrolysis of AB is to be accelerated by transition metal nanocatalysts [21,22]. In particular, the nanoparticles (NPs) of platinum [23], palladium [24], and rhodium [25] are found to be the highest activity catalysts in releasing $H_2$ from AB which can be used in pure hydrogen supply for on-board applications. Ruthenium is one of the most extensively tested noble metals for catalyzing the hydrolysis of AB [26]. Because of the relatively high price of ruthenium [27], the challenge is to increase its overall utilization efficiency in the hydrolytic dehydrogenation of AB. Although some water-soluble ruthenium complexes [28-30] are known to act as homogenous catalysts for releasing $H_2$ from AB, the colloidal ruthenium(0) NPs provide quite high activity for the same reaction at room temperature [31-38]. However, the instability of transition metal NPs against agglomeration greatly hampers their catalytic performance [39]. Therefore, ruthenium(0) NPs have

* Correspondence: sozkar@metu.edu.tr

been stabilized by anchoring them on a variety of supports with large surface area [21,40]. Thus, ruthenium(0) NPs have been anchored on carbonaceous materials with large surface area [41-63], oxide nanopowders such as silica [64-66], cobalt oxide [67,68], molybdenum oxide [69], perovskite [70], alumina [71-73], titania [74-76], zirconia [77], hafnia [78], ceria [79], and xonotlite [80] and confined in the pores of zeolite [81-84] and metal-organic frameworks [85-90]. Using reducible oxide supports has been shown to provide noticeably high turnover frequency (TOF) for the $Ru^0$ NPs in releasing $H_2$ from AB: TOF = 241 $min^{-1}$ on $TiO_2$ [76], 173 $min^{-1}$ on $ZrO_2$ [77], 170 $min^{-1}$ on $HfO_2$ [78], 361 $min^{-1}$ on $CeO_2$ [79], and 2114 $min^{-1}$ on $Co_3O_4$ [67]. $WO_3$ is another unique reducible oxide which can increase the catalytic activity of transition metal NPs in hydrolytic dehydrogenation [91,92]. Particularly, using the transition metal(0) NPs on the oxygen-deficient $WO_{3-x}$ can significantly increase the catalytic activity [93-96]. A 2019 paper [96] reports the use of rhodium(0) NPs on $WO_{3-x}$ nanowires as catalysts for the hydrolysis of AB though under visible light irradiation. For the hydrogen evolution from AB, a significant enhancement in catalytic activity of nickel nanocatalyst has been achieved through its coupling with $WO_{3-x}$ nanorods [97]. A very recent paper [98] reports the promotion effects of $WO_3$ on the catalytic activity of platinum(0) NPs in the same reaction. We have also reported the use of $WO_3$ as support for the rhodium(0) NPs in hydrogen evolution from AB [99]. The $Rh^0/WO_3$ nanocatalysts could be obtained by sodium borohydride reduction of rhodium(III) precursor impregnated on oxide powder. The resulting $Rh^0/WO_3$ (0.5% wt. Rh) nanocatalyst provides the highest TOF of 749 $min^{-1}$ in liberating 3 equivalent $H_2$ from the hydrolysis of AB at 25 °C [99]. The observed high catalytic activity is accredited to reducible nature of the oxide support. Herein, we report the use of $WO_3$ support for the ruthenium(0) NPs and the employment of $Ru^0/WO_3$ in releasing $H_2$ from AB. The $Ru^0/WO_3$ catalysts can be obtained by $NaBH_4$ reduction of ruthenium(III) precursor impregnated on the oxide support and provide high activity in releasing $H_2$ from AB.

## 2. Experimental

The sections on materials and instrumentation are given in Supplementary Information (SI).

### 2.1. Preparation of $Ru/WO_3$

In a beaker, 1.0 g of $WO_3$ was stirred with aqueous $RuCl_3.3H_2O$ (54.6 mg) in distilled $H_2O$ (100 mL) for 24 h at room temperature. Next, ruthenium(III) ions were reduced with aqueous $NaBH_4$ (mol $NaBH_4$/mol Ru = 3). The resulting $Ru^0/WO_3$ NPs were isolated by centrifugation (10 min at 8000 rpm). The solid precipitate was washed with distilled $H_2O$ (15 mL) and separated again by centrifugation. The catalyst was then dried under vacuum at 60 °C for 12 h and characterized by various analytical techniques. The ruthenium content of the sample was determined as 2.0% wt. by ICP-OES analysis. Note that $Ru^0/WO_3$ (1.0% wt. Ru) and $Ru^0/WO_3$ (3.0% wt. Ru) samples were also prepared following the same procedure as the one given above by using 26.56 mg and 84.18 mg of $RuCl_3.3H_2O$, respectively. The Ru contents of the obtained samples were also determined by ICP-OES to be 1.0% and 3.01% wt. Ru, respectively.

### 2.2. Determination of the most active Ru loading for $Ru/WO_3$ used in hydrolysis of AB

The catalytic activity of $Ru^0/WO_3$ (1.0% wt. Ru), $Ru^0/WO_3$ (2.0% wt. Ru), and $Ru^0/WO_3$ (3.0% wt. Ru) was tested in releasing $H_2$ from the hydrolysis of AB starting with 0.60 mM Ru and 100 mM AB in 10 mL solution at 25.0 ± 0.1 °C. The highest activity was achieved by using $Ru/WO_3$ (1.0% wt. Ru) which was used for all other tests.

### 2.3. Catalytic activity of $Ru/WO_3$ in hydrolysis of AB at various conditions

The hydrolysis reaction was investigated as described in our previously published procedure [99], which was provided in the SI file. The reaction was performed starting with 60.0 mg of $Ru/WO_3$ (1.0% wt. Ru) ([Ru] = 0.6 mM) in 10 mL $H_2O$ and AB (1.0 mmol) at different temperatures (20, 25, 30, 40 °C) in order to calculate the apparent activation energy. The catalytic activity of $Ru/WO_3$ (1.0% wt) was also tested at different weights (30.0, 60.0, 90.0, 120.0 mg) and thus with various ruthenium concentrations (0.3, 0.6, 0.9, 1.18 mM) at 25 °C.

### 2.4. Durability of $Ru/WO_3$ in hydrolysis of AB

Both recyclability and reusability of $Ru/WO_3$ (1.0% wt.) catalyst were investigated in hydrolysis of AB (100 mM AB in 10 mL of $H_2O$) at 25.0 °C. The recyclability and the reusability tests were performed using 120.0 mg and 160.0 mg of $Ru/WO_3$ (1.0% wt.) catalysts, respectively. For the former test, 1.0 mmol AB was transferred into the reactor for another run of the hydrolysis when the first run of hydrolysis was completed. For the latter test, the catalyst and the reaction solution were isolated by centrifugation after the first run. The isolated catalyst was redispersed in 10.0 mL of $H_2O$ in the reaction vessel and a new batch of AB was transferred into this mixture and the second run of the hydrolysis reaction was started again. The same procedure was followed after the second run, third run, and forth run. Note that bare $WO_3$ provides no activity in the hydrolysis reaction.

## 3. Results and discussion

Ruthenium(0) NPs supported on tungsten(VI) oxide powder were successfully prepared from the reduction of $Ru^{3+}$ ions on the surface of support by sodium borohydride. The ruthenium contents of the obtained three $Ru^0/WO_3$ samples were

determined by ICP and found to be 1.0%, 2.03%, and 3.01% wt. Ru which were very close to the theoretical values and similar to the values obtained by the EDX surface analysis (vide infra). Consequently, the three samples are denoted as $Ru^0/WO_3$ (1.0% wt. Ru), $Ru^0/WO_3$ (2.0% wt. Ru), and $Ru^0/WO_3$ (3.0% wt. Ru). The obtained $Ru^0/WO_3$ catalysts were characterized by TEM, XRD, FE-SEM, XPS, and EDX techniques. A comparison of XRD patterns of the bare $WO_3$ and $Ru^0/WO_3$ samples (Figure 1) indicates that the tungsten(VI) oxide support retains its crystallinity and integrity after the impregnation and reduction of ruthenium(III) ions on the surface; that is, after the ruthenium loading. Note that no diffraction peak is observed for the ruthenium(0) NPs because of the low loading (<3.0% wt. Ru).

TEM-EDX (Figure 2), FE-SEM electron mapping (Figure 3), and survey scan XPS (Figure 4) analyses confirm the presence of $Ru^0$ NPs well dispersed on the surface of tungsten(VI) oxide support. Furthermore, they show that the sole elements existent in the sample are ruthenium, tungsten, and oxygen. The TEM image of $Ru^0/WO_3$ nanocatalyst with 1.0% wt. Ru loading (Figure 2a) shows the presence of highly dispersed ruthenium(0) NPs on the $WO_3$ support. The histogram in Figure 2b shows the particle size distribution in the range 1.5–4.0 nm with a mean diameter of 2.6 nm.XPS was used to investigate the elemental composition of $Ru^0/WO_3$ (1.0% wt. Ru) nanocatalyst as well as the oxidation state of Ru NPs. A survey scan XPS analysis confirms the existence of only O, W, and Ru elements (Figure 4a). High-resolution scans of Ru 3p and Ru 3d XPS are displayed in Figures 4b and 4d, respectively. The Ru $3d_{3/2}$ peak in Figure 4d unfortunately overlaps with C 1s peak which makes the analysis difficult. High resolution scan Ru 3p XPS in Figure 4b exhibits two intense peaks at 462.6 and 485 eV which are ascribed to the ruthenium(0) $3p_{3/2}$ and $3p_{1/2}$ bands, respectively [100,101].

Since the $Ru^0$ $3p_{1/2}$ and W $4p_{1/2}$ peaks overlap with each other, we could analyze only the $Ru^0$ $3p_{3/2}$ peak in Figure 4c which shows its deconvolution to two well-resolved peaks at 461.7 and 463.5 eV. The higher energy peak at 463.5 eV is assigned to a ruthenium(0) species with slightly higher partial positive charge than the other ruthenium(0) species giving rise to the lower energy peak at 461.7 eV [102]. The observation of two $Ru^0$ $3p_{3/2}$ peaks in Figure 4c implies the presence of two different ruthenium atoms in ruthenium(0) NPs. These two ruthenium(0) species differ from each other by the

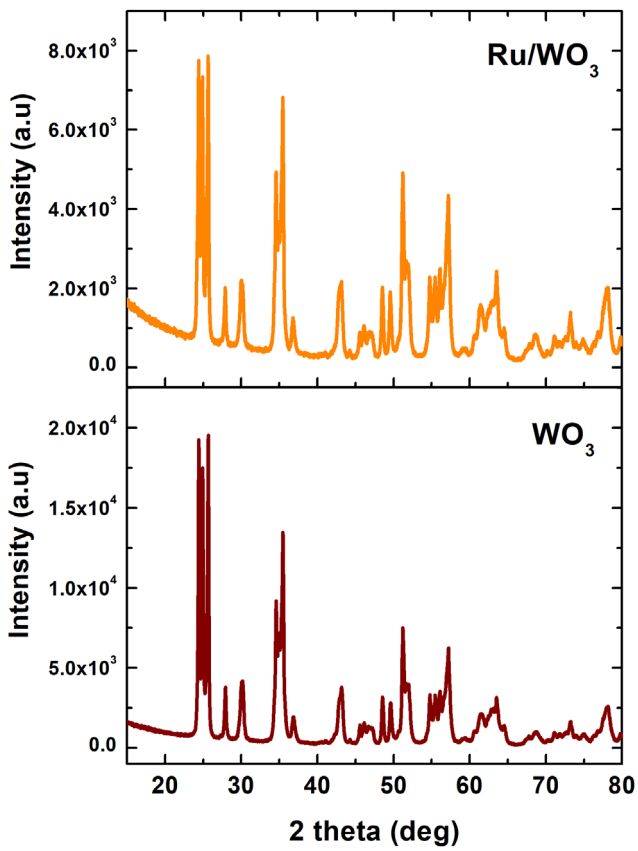


**Figure 1**. XRD pattern of $WO_3$ support and $Ru^0/WO_3$ (1.0% wt. Ru) NPs.

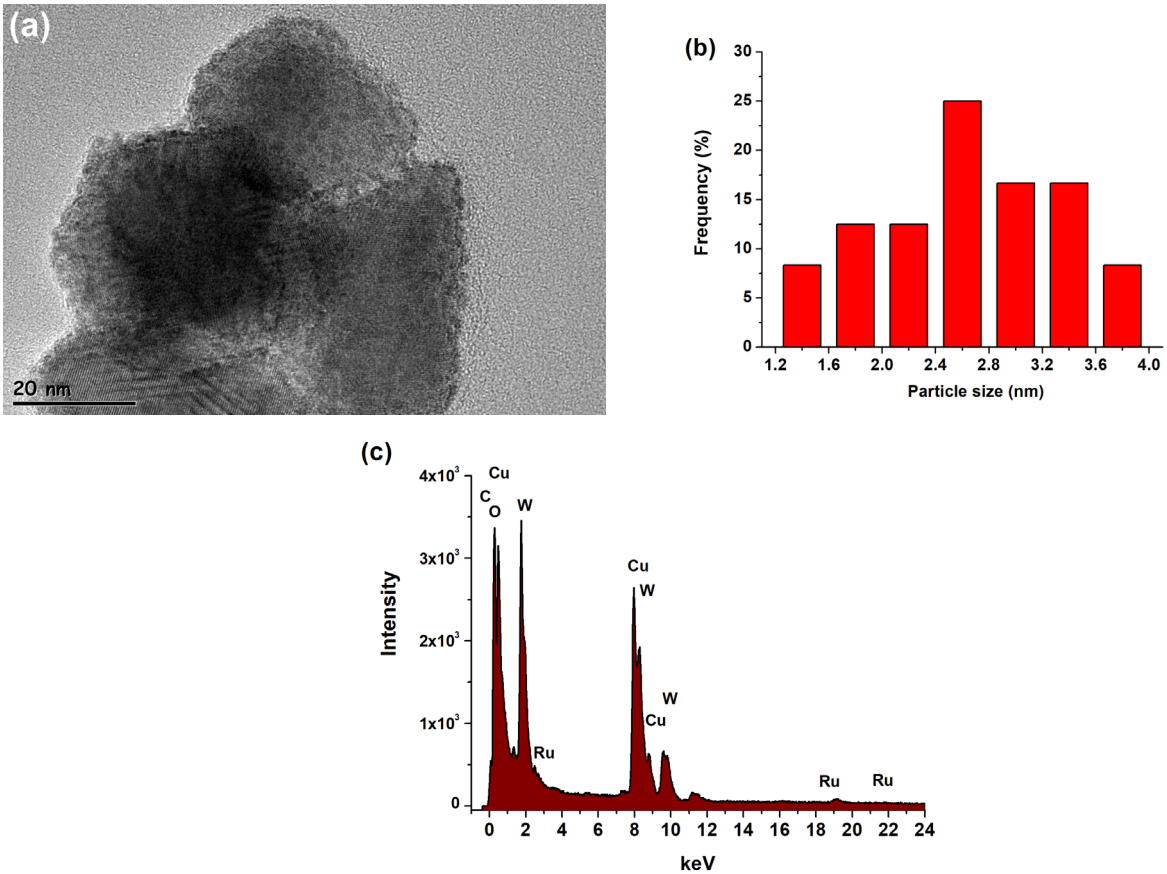


**Figure 2**. (a) TEM image, (b) histogram for the size distribution, and (c) TEM-EDX spectrum for $Ru/WO_3$ (1.0% wt. Ru).

extend of interaction with the reduced tungsten oxide support. Indeed, the high resolution scan W 4f XPS in Figure 4e gives an undeniable evidence for the reduction of tungsten oxide support as it shows two prominent intense peaks for tungsten(VI) which are readily ascribed to the $W^{6+}$ $4f_{7/2}$ and $4f_{5/2}$ bands [103] and more importantly, two weak intensity peaks (recognized by deconvolution) belong to the $W^{5+}$ $4f_{7/2}$ and $4f_{5/2}$ bands [104]. Note that the peaks at 34.9 and 37.1 eV are ascribed to $W^{6+}$ while the other two weak intensity peaks at 34.2 and 36.4 eV are assigned to the $W^{5+}$ in Figure 4e. The observation of two peaks for the tungsten(V) species explains the color change observed for the oxide support under the reducing conditions (vide infra).

The $WO_3$ support changes its color from light green to blue under the reducing conditions, that is, in the presence of reducing agent (sodium borohydride or ammonia borane). Observation of color change indicates the fractional reduction of tungsten(VI) to tungsten(V) which is demonstrated by the high resolution W 4f XPS in Figure 4e as reported previously [99]. The fractional reduction causes a negative charge building up on the support surface which can affect catalytic activity of ruthenium(0) NPs. Furthermore, the high resolution Ru $3p_{3/2}$ XPS in Figure 4c exhibits the presence of two kinds of putative ruthenium(0): The one at higher binding energy of 463.5 eV has slightly higher partial positive charge than the other at 461.7 eV. Nearly spherical NPs on the tungsten oxide surface have essentially two kinds of ruthenium atoms; the first kind of ruthenium atoms is in contact with the oxide surface, the second kind is free and does not interact directly with the surface. The reduced tungsten oxide may cause negative charge on the support surface which interacts with the ruthenium atoms in contact with the oxide surface. Charge transfer occurs from ruthenium metal to oxide surface in this metal-support interaction. Thus, the ruthenium atoms of the first kind, which are in direct contact with the support, gain higher partial positive charge through the interaction with the oxide surface than the second kind as shown by the XPS. Hence, the strong interaction between the reducible $WO_3$ and ruthenium(0) NPs has an influence on both the stability and activity of $Ru^0/WO_3$ nanocatalyst in releasing 3 equivalent $H_2$ per mole of AB in hydrolysis.

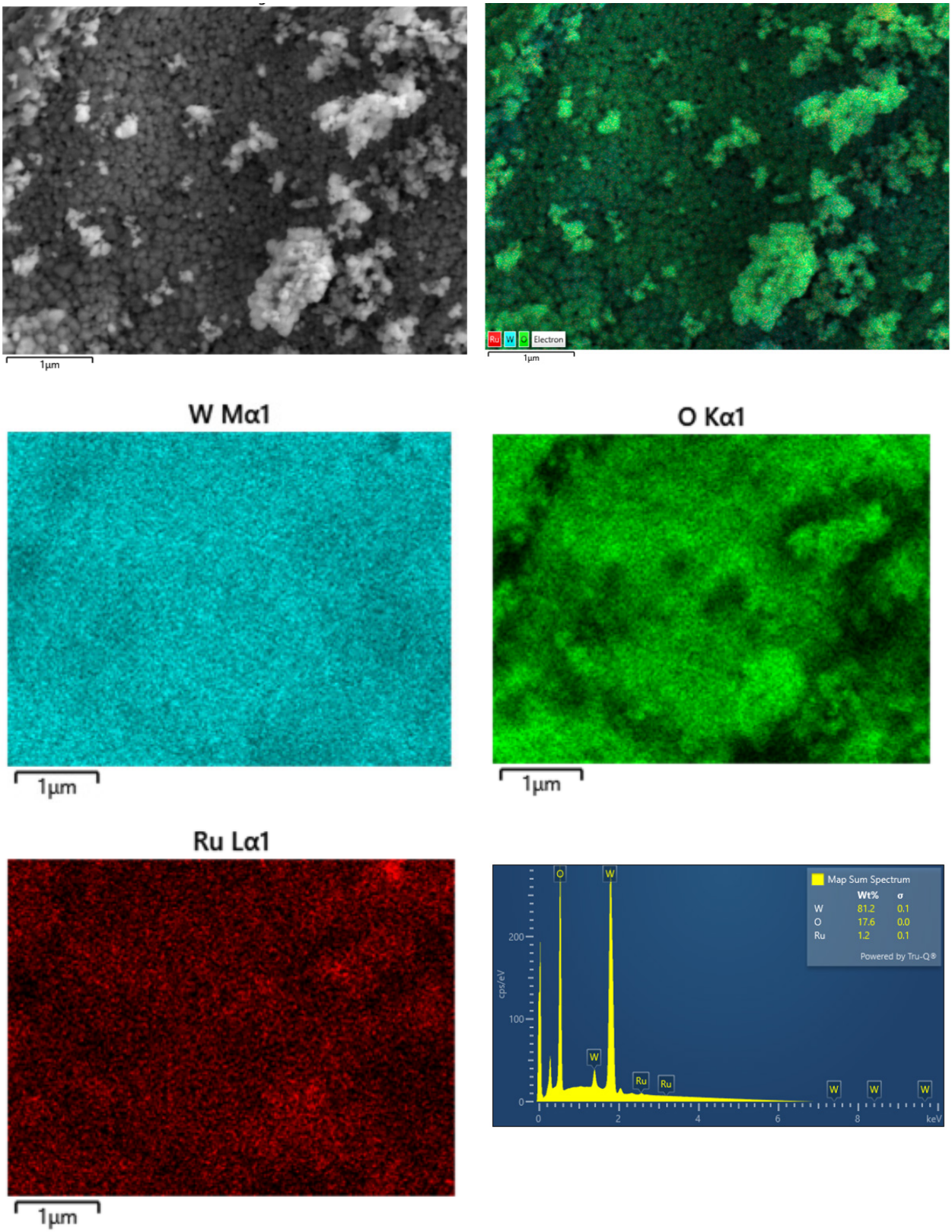


**Figure 3**. FE-SEM mapping and EDS of $Ru/WO_3$ (1.0% wt. Ru) sample. Note that cyan, green, and red colors on the images obtained by electron mapping show W, O, and Ru elements, respectively.

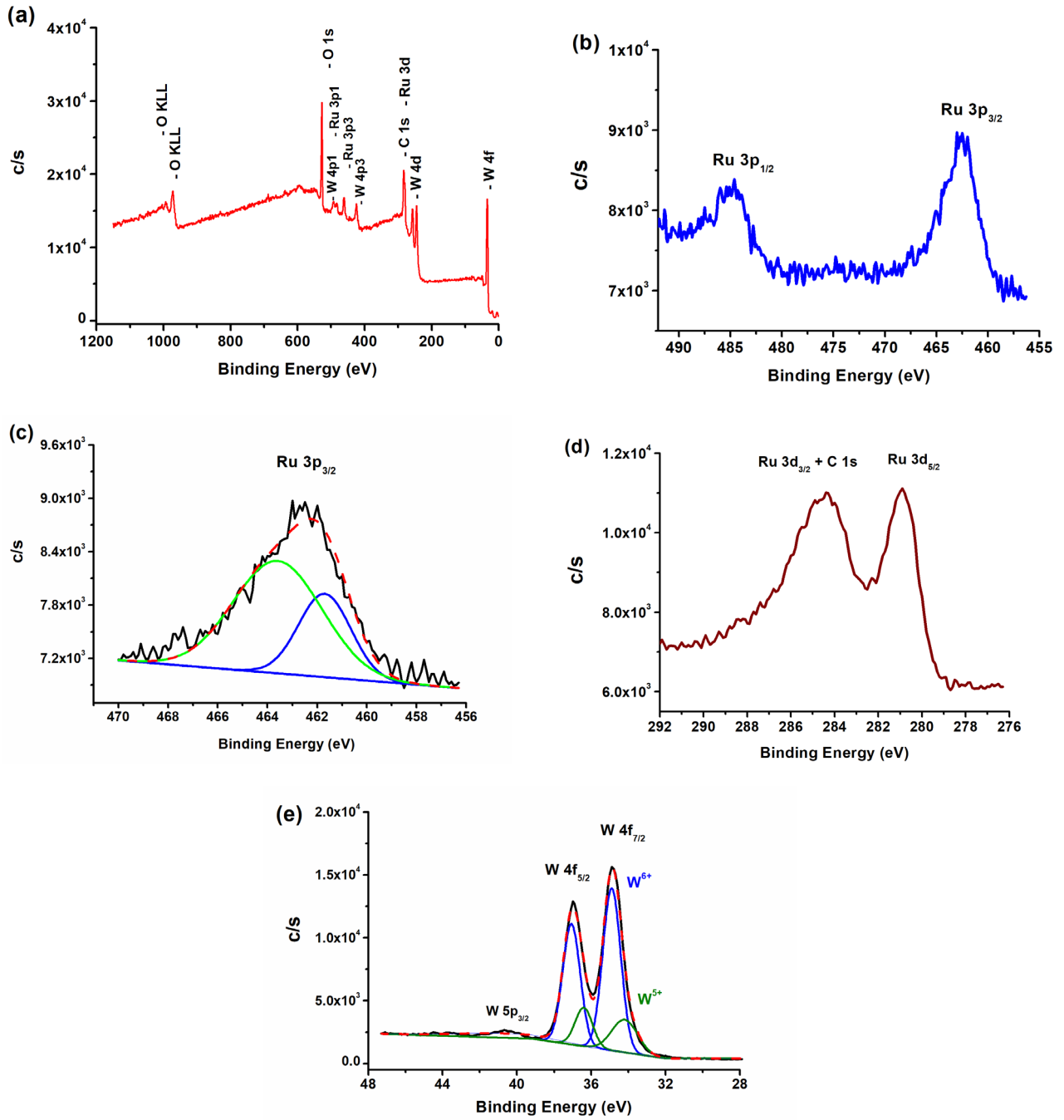


**Figure 4**. XPS spectra of the $Ru^0/WO_3$ (1.0% wt. Ru) nanocatalyst: (a) Survey scan, (b) high-resolution Ru 3p, (c) high-resolution Ru $3p_{3/2}$, (d) high-resolution Ru 3d, and (e) high-resolution W 4f.

Catalytic activity of $Ru^0/WO_3$ NPs with different ruthenium contents was tested in $H_2$ generation from the hydrolysis of AB. Figure 5 shows the hydrogen generation plots for the hydrolysis of AB (100 mM) at 25.0 °C performed starting with $Ru^0/WO_3$ NPs of three different ruthenium loadings (1.0%, 2.0%, and 3.0% wt. Ru). The $H_2$ generation starts immediately and lasts almost linearly until the end of hydrolysis releasing 3 equivalent $H_2$ per mole of AB. The immediate start of hydrogen evolution indicates that the catalyst is preformed by borohydride reduction of precursor. TOF values can be computed

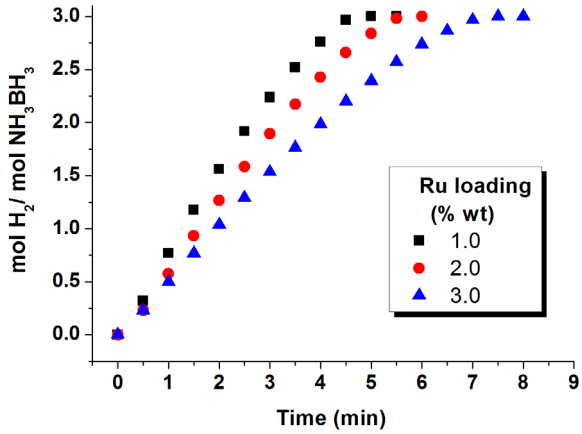


**Figure 5.** Hydrogen evolution plots (equivalent $H_2$ per mole of AB versus time) for the hydrolytic dehydrogenation of ammonia borane starting with $Ru^0/WO_3$ NPs at different ruthenium loadings at 25.0 ± 1.0 °C. [Ru] = 0.6 mM and [AB] = 100 mM.

from the linear portion of hydrogen evolution plots using the formula given in the experimental section (SI). The TOF values of $Ru^0/WO_3$ nanocatalysts with ruthenium contents of 1.0%, 2.0%, and 3.0% are 122, 106, and 83 $min^{-1}$, respectively, for the release of 3 equivalent $H_2$ per mole of AB in hydrolysis at 25.0 °C. As expected, the catalytic activity decreases with the increasing metal content [105]. Since the $Ru^0/WO_3$ (1.0% wt. Ru) nanocatalyst shows the maximum activity, it was used for all the other hydrolysis experiments in the present study. The TOF value of $Ru^0/WO_3$ (1.0% wt. Ru) nanocatalyst is found to be comparable to the ones of the ruthenium(0) NPs on the surface of other oxide supports listed in Table.

Figure 6 shows hydrogen evolution plots recorded during AB hydrolysis starting with $Ru^0/WO_3$ (1.0% wt. Ru) nanocatalyst in various catalyst weight at 25.0 °C. Hydrogen generation rate was determined from the slope of each plot in the linear portion (Figure 6a) and charted vs. ruthenium concentration, both in logarithmic scale. This gives a straight line with a slope of 0.9 specifying that the hydrolysis reaction of AB catalyzed by $Ru/WO_3$ (1.0% wt. Ru) NPs is first order with respect to concentration of the ruthenium catalyst (Figure 6b). Since the hydrogen generation occurs linearly almost until the end in all of the hydrogen generation plots, one can conclude that the hydrolysis reaction is zero order with respect to AB concentration.

Hydrolysis reaction of AB was also performed at various temperatures using $Ru/WO_3$ (1.0% wt. Ru) nanocatalyst (Figure 7a), where rate constants for the $H_2$ evolution were determined from the slope in linear part. The temperature-dependent rate constants could be evaluated by constructing the Arrhenius graph in Figure 7b to calculate the apparent activation energy to be $E_a$ = 77 ± 2 kJ $mol^{-1}$ for AB hydrolysis using $Ru^0/WO_3$ (1.0% wt. Ru).

The durability and stability of nanocatalysts can be measured by percentage of the retained initial activity in the consecutive recyclability and reusability tests, respectively. The recyclability check is implemented by addition of a new batch of substrate to the reaction solution after complete hydrolysis in the present run without isolation of catalyst. For testing the reusability of nanocatalysts in AB hydrolysis, the catalyst needs to be isolated from the solution after the completion of reaction and then, placed in a new reactor with new batch of substrate for the following run of hydrolysis. The initial activity retained in each run is recorded and given in percentage [106]. Figure 8 displays the scores of recyclability and reusability tests for the $Ru^0/WO_3$ (1.0% wt. Ru) nanocatalyst. The results of recyclability test in Figures 8a and 8c reveal that the catalyst retains only 67% of initial activity after the 5th cycle. The activity loss during the consecutive cycles is due to deactivation by metaborate ions which are accumulated during the whole reaction. Figures 8b and 8d show the results of reusability tests performed by isolating and then redispersing nanocatalyst in a new AB batch for the next run. There is no activity loss in successive runs. A noteworthy observation is that activity increases on passing from the first run to the second and then to the third run. Then it remains constant. Furthermore, the isolated solution after each run of reusability exhibits no catalytic activity in the hydrolysis of AB, which demonstrates the absence of leaching of ruthenium from the support to the reaction solution. The increase in catalytic activity on going from the first to the third run is likely due to

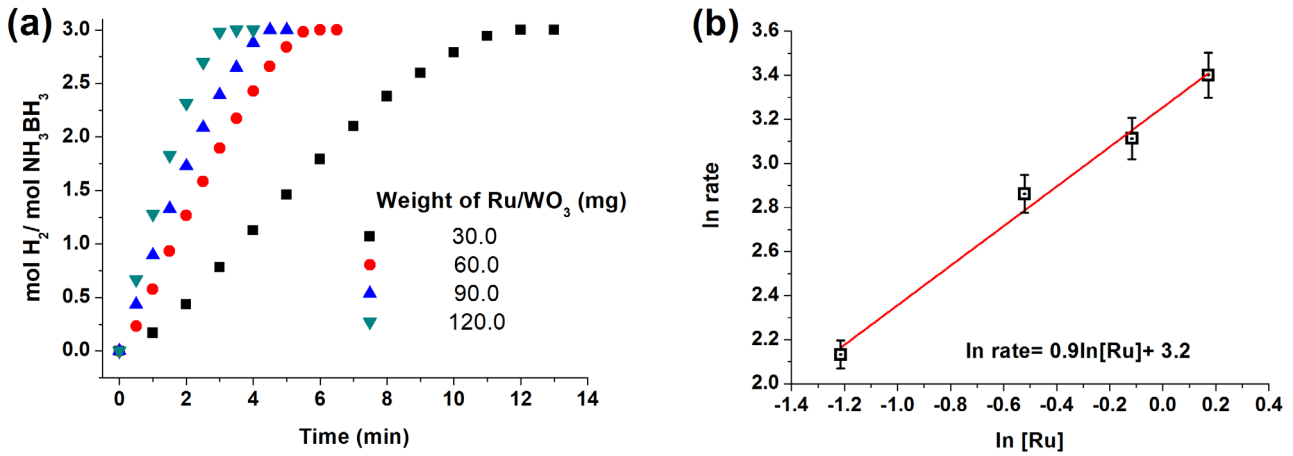


**Figure 6.** (a) Hydrogen generation plots (mol $H_2$/mol $H_3N.BH_3$ versus time) for $Ru^0/WO_3$ NPs depending on catalyst weight in hydrolysis of AB (100 mM) at 25.0 ± 0.1 °C. (b) Hydrogen generation versus ruthenium concentration plot, both axes in logarithmic scale.

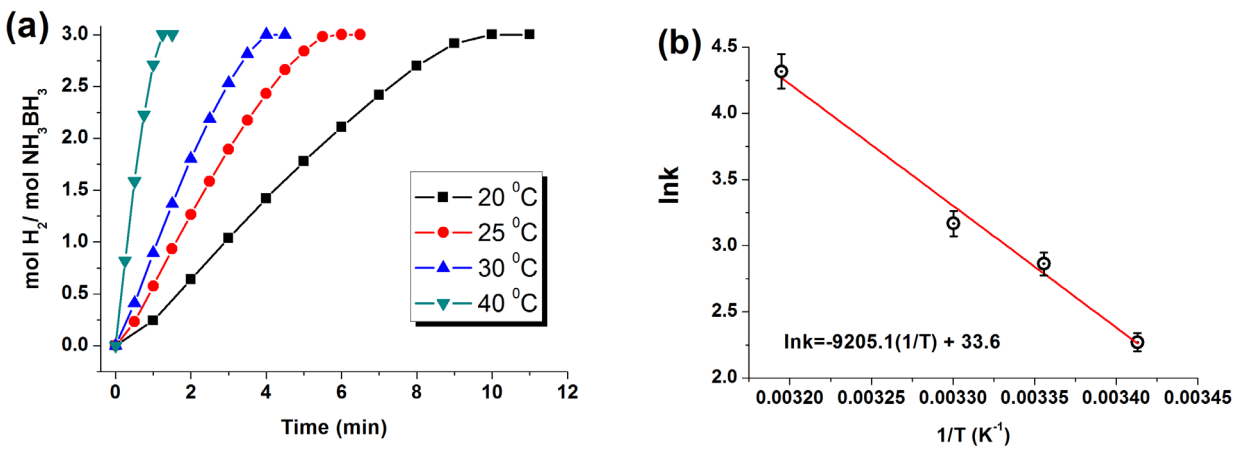


**Figure 7.** (a) Hydrogen generation plots (mol $H_2$ per mole of AB vs. time) during the hydrolysis reaction at various temperatures starting with $Ru^0/WO_3$ (1.0% wt. Ru). [Ru] = 0.60 mM, [AB] = 100 mM. (b) Arrhenius plot for AB hydrolysis catalyzed by $Ru^0/WO_3$ (1.0% wt. Ru).

the continuing formation of $Ru^0$ NPs by in situ reduction of ruthenium in higher oxidation state which might be formed by air exposure during the isolation and redispersing procedure.

The activity and reusability of ruthenium catalysts plus activation energies for the hydrolytic dehydrogenation of ammonia borane including the ones reported in the previously uncited papers [107-114] are listed in Table. $Ru^0/WO_3$ (1.0% wt. Ru) nanocatalyst provides a descent activity in releasing $H_2$ from AB as compared to the literature values. Another noteworthy observation is that there is no correlation between the activation energy and catalytic activity in contrast to the general belief that the decreasing activation energy would correlate with the increasing catalytic activity.

## 4. Conclusions

$Ru^0/WO_3$ (1.0% wt. Ru) nanocatalyst with a mean diameter of 2.6 nm provides descent activity in releasing $H_2$ from the hydrolysis of ammonia borane at room temperature, and more importantly, it appears to be reusable as the catalyst retains 100% of initial activity in the fifth run of hydrolysis. Since no leaching is observed for the ruthenium(0) NPs from the oxide surface to the solution, there exists conceivably a strong metal-support interaction between the ruthenium and tungsten oxide. The XPS analyses yield results supporting such a strong interaction between the ruthenium(0) NPs and the reduc-

**Table.** Apparent activation energy ($E_a$) and TOF values for ruthenium-based catalysts reported for AB hydrolysis at 25 °C. *where catalyst was isolated from reaction medium after each of successive run for the next use.

| **Catalyst** | **TOF ($min^{-1}$)** | **$E_a$ ($kJ\ mol^{-1}$)** | **Reusability % activity retained** | **Ref.** |
|---|---|---|---|---|
| Ru NPC | 813 | 25 | *67.3% in 5 run | 107 |
| Ru/graphene | 600 | 13 | 80% in 5 cycle | 48 |
| Ru/graphene | 100 | 12 | 72% in 4 cycle | 49 |
| Ru/carbon black | 430 | 35 | *43.1% in 5 run | 47 |
| Ru/AC | 235 | 68 | 100% in 5 cycle | 45 |
| Ru/MWCNT | 329 | 33 | *41% in 4 run | 43 |
| Ru/g-$C_3N_4$ | 313 | 37 | *50% in 4 run | 62 |
| Ru/nanodiamond | 229 | 51 | *40% in 5 run | 60 |
| Commercial Ru/C | 113 | 76 | - | 108 |
| Nanoporous Ru | 27 | 67 | 67% in 5 cycle | 109 |
| Ru/γ-$Al_2O_3$ | 88 | 29 | - | 73 |
| Ru/$SiO_2$ | 200 | 38 | - | 65 |
| Ru/$SiO_2$-$CoFe_2O_4$ | 173 | 46 | *94% in 10 run | 66 |
| Ru/$SiO_2$-$Fe_3O_4$ | 127 | 54 | *100% in 5 run | 110 |
| Ru/$TiO_2$ nanotube | 303 | 46 | 25% in 4 cycle | 74 |
| Ru/$TiO_2$ | 241 | 70 | 100% in 3 cycle | 76 |
| Ru/$TiO_2$ (anatase) | 200 | 87 | 65% in 5 cycle | 75 |
| Ru/$TiO_2$ (anatase+rutile) | 604 | 38 | - | 111 |
| Ru/$ZrO_2$ | 173 | 58 | *67% in 5 run | 77 |
| Ru/$HfO_2$ | 170 | 65 | *75% in 5 run | 78 |
| Ru/$CeO_2$ | 361 | 51 | *60% in 5 run | 79 |
| Ru@S1B-10C | 202 | 24 | 70% in 5 cycle | 83 |
| Ru/SBA-15 | 316 | 35 | 100% in 5 cycle | 84 |
| Ru-MIL 53 (Al) | 267 | 34 | 75% in 4 cycle | 86 |
| Ru-MIL 53 (Cr) | 261 | 29 | 71% in 4 cycle | 86 |
| Ru/MCM-41 | 288 | 42 | 75% in 5 cycle | 90 |
| Ru-MIL 96 | 231 | 48 | 65% in 5 cycle | 88 |
| Ru-MIL-101 | 178 | 51 | - | 112 |
| Ru/HAP | 137 | 58 | *92% in 5 run | 113 |
| Ru/X-NW | 135 | 77 | - | 80 |
| Ru@ZK-4 | 90 | 28 | *85% in 5 run | 114 |
| $Ru^0/WO_3$ | 122 | 27 | *100% in 5 run | This study |

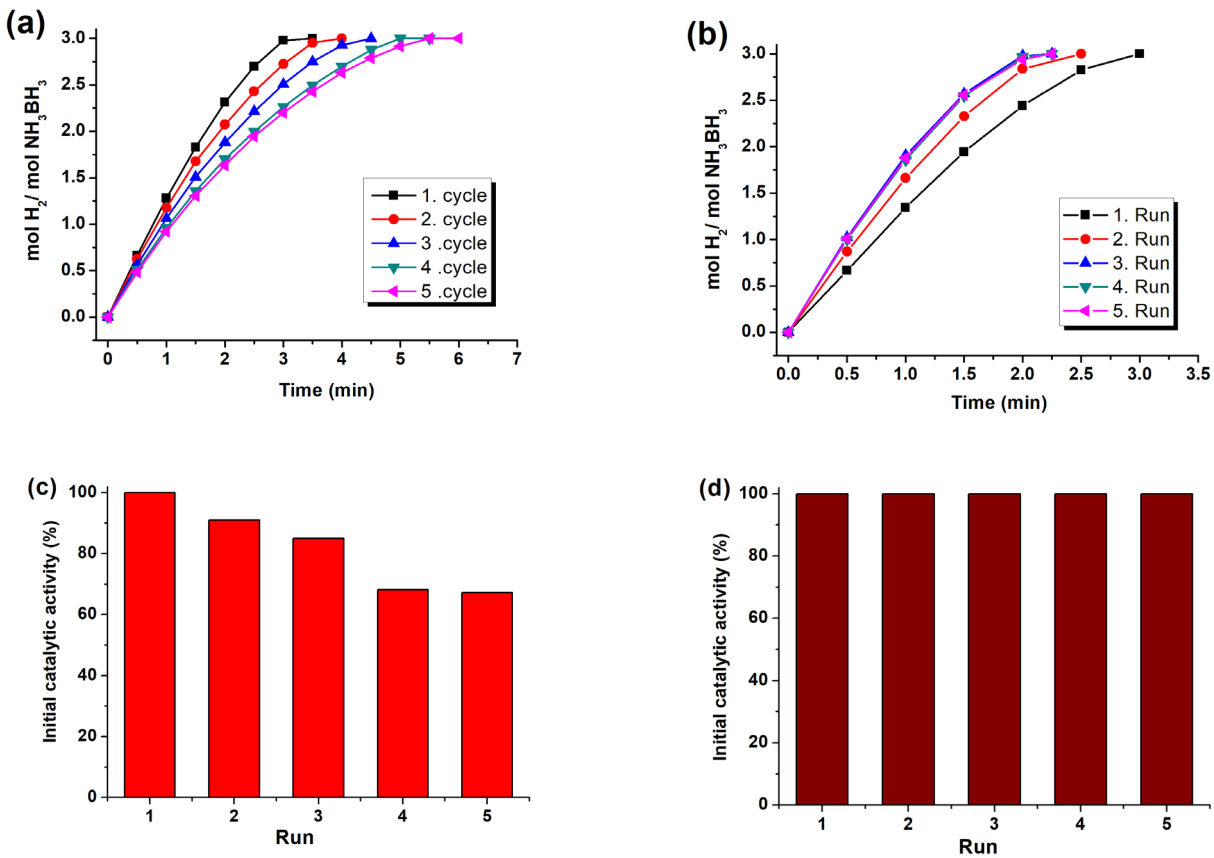


**Figure 8.** Hydrogen generation plots (mol $H_2$ per mole of AB vs. time) in catalytic hydrolysis of AB (100 mM) starting with (a) $Ru^0/WO_3$ (1.18 mM Ru) and (b) $Ru^0/WO_3$ (1.58 mM Ru) from the first to the fifth run at 25.0 °C. Percent initial activity retained in use for (c) the recyclability and (d) the reusability test.

ible tungsten oxide surface.

The $Ru^0/WO_3$ (1.0% wt. Ru) nanocatalyst exhibits unusually high stability. Usually, such a high reusability can be achieved by the magnetically isolable NPs [25], as the nanocatalyst can readily be recovered using an exterior magnet. Although the nonmagnetic $Ru^0/WO_3$ nanocatalysts need to be isolated by filtration or centrifugation, no activity loss is observed even after the 5th run of hydrolysis. Hence, this high reusability of $Ru^0/WO_3$ nanocatalysts can make a noticeable contribution to the utilization efficiency of precious ruthenium in catalyzing the hydrolytic dehydrogenation of ammonia borane.

**Acknowledgments**

Partial support by Turkish Academy of Sciences is acknowledged. This work has been supported by Necmettin Erbakan University Scientific Research Projects Coordination Unit, Project numbers: 2112MER03003, 221219006

## References

[1] Nejat P, Jomehzadeh F, Taheri MM, Gohari M, Majid MZA. A global review of energy consumption, $CO_2$ emissions and policy in the residential sector (with an overview of the top ten $CO_2$ emitting countries). Renewable Sustainable Energy Rev. 2015; 43: 843-862. https://doi.org/10.1016/j.rser.2014.11.066

[2] Okafor C, Madu C, Ajaero C, Ibekwe J, Bebenimibo H et al. Moving beyond fossil fuel in an oil-exporting and emerging economy: Paradigm shift. AIMS Energy. 2021; 9: 379-413. https://doi.org/10.3934/energy.2021020

[3] Overpeck JT, Cole JE. Abrupt change in Earth's climate system. Annu Rev Environ Resour. 2006; 31:1-31. https://doi.org/10.1146/annurev.energy.30.050504.144308

[4] Anderson TR, Hawkins E, Jones PD. $CO_2$, the greenhouse effect and global warming: from the pioneering work of Arrhenius and Callendar to today's Earth System Models. Endeavour. 2016; 40: 178-187. https://doi.org/10.1016/j.endeavour.2016.07.002

[5] Oreskes N. The scientific consensus on climate change. Science. 2004; 306: 1686. https://doi.org/10.1126/science.1103618

[6] Uyar TS, Besikci D. Integration of hydrogen energy systems into renewable energy systems for better design of 100% renewable energy communities. International Journal of Hydrogen Energy 2017; 42:2 453-2456. https://doi.org/10.1016/j.ijhydene.2016.09.086

[7] Armaroli N, Balzani V. The hydrogen issue. ChemSusChem 2011; 4: 21–36. https://doi.org/10.1002/cssc.201000182

[8] Karakaya E, Nuur C, Assbring L. Potential transitions in the iron and steel industry in Sweden: towards a hydrogen-based future? Journal of Cleaner Production 2018; 195: 651-663. https://doi.org/10.1016/j.jclepro.2018.05.142

[9] He T, Pachfule P, Wu H, Xu Q, Chen P. Hydrogen carriers, Nature Reviews Materials 2016; 1: 1-17. https://doi.org/10.1038/natrevmats.2016.59

[10] Otto A, Robinius M, Grube T, Schiebahn S, Praktiknjo A et al. Power-to-steel: reducing $CO_2$ through the integration of renewable energy and hydrogen into the German steel industry. Energies. 2017; 10: e451. https://doi.org/10.3390/en10040451

[11] Dresselhaus MS, Thomas IL. Alternative energy technologies. Nature. 2001; 414: 332-337.

[12] Demirci UB, Ammonia Borane: An extensively studied, though not yet implemented, hydrogen carrier. Energies. 2020; 13: e3071. https://doi.org/10.3390/en13123071

[13] Demirci, UB. Ammonia borane, a material with exceptional properties for chemical hydrogen storage. International Journal of Hydrogen Energy 2017; 42: 9978-10013. https://doi.org/10.1016/j.ijhydene.2017.01.154

[14] Petit JF, Miele P, Demirci UB. Ammonia borane $H_3N$-$BH_3$ for solid-state chemical hydrogen storage: Different samples with different thermal behaviors. International Journal of Hydrogen Energy 2016; 41: 15462-15470. https://doi.org/10.1016/j.ijhydene.2016.06.097

[15] Akbayrak S, Özkar S. Ammonia borane as hydrogen storage materials. International Journal of Hydrogen Energy. 2018: 43; 18592-18606. https://doi.org/10.1016/j.ijhydene.2018.02.190

[16] Chandra M, Xu Q. A high-performance hydrogen generation system: Transition metal-catalyzed dissociation and hydrolysis of ammonia-borane. Journal of Power Sources. 2006; 156: 190-194. https://doi.org/10.1016/j.jpowsour.2005.05.043

[17] Xu Q, Chandra M. Catalytic activities of non-noble metals for hydrogen generation from aqueous ammonia–borane at room temperature. Journal of Power Sources. 2006; 163: 364–370. https://doi.org/10.1016/j.jpowsour.2006.09.043

[18] Sanyal U, Demirci UB, Jadirgar BR, Miele P. Hydrolysis of ammonia borane as a hydrogen source: fundamental issues and potential solutions towards implementation, ChemSusChem. 2011; 4: 1731–1739. https://doi.org/10.1002/cssc.201100318

[19] Brockman A, Zheng Y, Gore J. A study of catalytic hydrolysis of concentrated ammonia borane solutions. International Journal of Hydrogen Energy 2010; 35: 7350-7356. https://doi.org/10.1016/j.ijhydene.2010.04.172

[20] Basu S, Zheng Y, Varma A, Delgass WN, Gore JP. Catalytic hydrolysis of ammonia borane: Intrinsic parameter estimation and validation. Journal of Power Sources 2010; 195: 1957-1963. https://doi.org/10.1016/j.jpowsour.2009.10.070

[21] Zahmakiran M, Özkar S. Metal NPs in liquid phase catalysis; from recent advances to future goals. Nanoscale. 2011; 3: 3462-3481. https://doi.org/10.1039/C1NR10201J

[22] Zahmakiran M, Özkar S. Transition metal NPs in catalysis for the hydrogen generation from the hydrolysis of ammonia-borane. Topics in Catalysis. 2013; 56: 1171-1183. https://doi.org/10.1007/s11244-013-0083-5

[23] Özkar S. A review on platinum(0) nanocatalysts for hydrogen generation from the hydrolysis of ammonia borane. Dalton Trans. 2021; 50: 12349-12364. https://doi.org/10.1039/D1DT01709H

[24] Akbayrak S, Özkar S. Magnetically isolable $Pd^0/Co_3O_4$ nanocatalyst: Exceptionally high catalytic activity and outstanding reusability in releasing $h_2$ from the hydrolysis of ammonia borane. Journal of Colloid and Interface Science 2022; 626: 752-758. https://doi.org/10.1016/j.jcis.2022.06.135

[25] Tonbul Y, Akbayrak S, Özkar S. Magnetically Separable Rhodium NPs as Catalysts for Releasing Hydrogen from the Hydrolysis of Ammonia Borane. Journal of Colloid and Interface Science 2019; 553: 581–587. https://doi.org/10.1016/j.jcis.2019.06.038

[26] Zhan WW, Zhu QL, Xu Q. Dehydrogenation of AB by metal nanoparticle catalysts. ACS Catalysis 2016; 6: 6892-6905. https://doi.org/10.1021/acscatal.6b02209

[27] The price change of precious metals including ruthenium can be followed using the link: https://pmm.umicore.com/en/prices/ruthenium/

[28] Boulho C, Djukic JP. The dehydrogenation of ammonia–borane catalysed by dicarbonylruthenacyclic(II) complexes. Dalton Transactions 2010; 39: 8893-8905. https://doi.org/10.1039/C0DT00241K

[29] Muñoz-Olasagasti M, Telleria A, Pérez-Miqueo J, Garralda MA, Freixa Z. A readily accessible ruthenium catalyst for the solvolytic dehydrogenation of amine–borane adducts. Dalton Transactions 2014; 43: 11404–11409. https://doi.org/10.1039/C4DT01216J

[30] Nacianceno VS, Garralda MA, Matxain JM, Freixa Z. Proton-responsive ruthenium(ii) catalysts for the solvolysis of ammonia-borane. Organometallics 2020; 39: 1238−1248. https://doi.org/10.1021/acs.organomet.0c00032

[31] Metin Ö, Sahin, S, Özkar, S. Water-soluble poly(4-styrenesulfonic acid-co-maleic acid) stabilized nanoclusters as highly active catalysts in hydrogen generation from the hydrolysis of ammonia borane. International Journal of Hydrogen Energy 2009; 34: 6304-6313. https://doi.org/10.1016/j.ijhydene.2009.06.032

[32] Durap F, Zahmakiran M, Özkar S. Water soluble laurate-stabilized ruthenium(0) nanoclusters catalyst for hydrogen generation from the hydrolysis of ammonia borane: High activity and long lifetime. International Journal of Hydrogen Energy 2009; 34: 7223-7230. https://doi.org/10.1016/j.ijhydene.2009.06.074

[33] Liu CH, Wu YC, Chou CC, Chen BH, Hsueh CL et al. Hydrogen generated from hydrolysis of using cobalt and ruthenium based catalysts. International Journal of Hydrogen Energy 2012; 37: 2950-2959. https://doi.org/10.1016/j.ijhydene.2011.05.022

[34] Rakap M. Hydrogen generation from hydrolysis of ammonia borane in the presence of highly efficient poly(N-vinyl-2- pyrrolidone)-protected platinum-ruthenium NPs. Applied Catalysis A General 2014; 478: 15-20. https://doi.org/10.1016/j.apcata.2014.03.022

[35] Abo-Hamed EK, Pennycook T, Vaynzof Y, Toprakcioglu C, Koutsioubas A et al. Highly Active Metastable NPs for Hydrogen Production through the Catalytic Hydrolysis of Ammonia Borane. Small 2014; 10: 3145-3152. https://doi.org/10.1002/smll.201303507

[36] Durap F, Caliskan S, Özkar S, Karakas K, Zahmakiran M. Dihydrogen phosphate stabilized ruthenium(0) NPs: efficient nanocatalyst for the hydrolysis of ammonia borane at room temperature. Materials 2015; 8: 4226. https://doi.org/10.3390/ma8074226

[37] Wang Q, Fu F, Escobar A, Moya S, Ruiz J et al. Click dendrimer-stabilized nanocatalysts for efficient hydrogen release upon hydrolysis of ammonia borane. ChemCatChem 2018; 10: 2673-2680. https://doi.org/10.1002/cctc.201800407

[38] Xu C, Wang H, Wang Q, Wang Y, Zhang Y et al. Ruthenium coordinated with triphenylphosphine-hyper-crosslinked polymer: An efficient catalyst for hydrogen evolution reaction and hydrolysis of ammonia borane. Applied Surface Science 2019; 466: 193-201. https://doi.org/10.1016/j.apsusc.2018.10.051

[39] Özkar S, Finke RG. Nanocluster formation and stabilization fundamental studies: ranking commonly employed anionic stabilizers via the development, then application of five comparative criteria. Journal of American Chemical Society 2002; 124: 5796-5810. https://doi.org/10.1021/ja012749v

[40] Özkar S. Enhancement of catalytic activity by increasing surface area in heterogeneous catalysis. Applied Surface Science 2009; 256: 1272-1277. https://doi.org/10.1016/j.apsusc.2009.10.036

[41] Wu Z, Duan Y, Ge S, Yip ACK, Yang F et al. Promoting hydrolysis of ammonia borane over multiwalled carbon nanotube-supported Ru catalysts via hydrogen spillover. Catalysis Communications 2017; 91: 10-15. https://doi.org/10.1016/j.catcom.2016.12.007

[42] Guo A, Hu L, Peng Y, Wang Y, Long Y et al. Steam pretreatment-mediated catalytic activity modulation for nanoclusters on nitrogen/oxygen-rich carbon nanotubes. Applied Surface Science 2022; 579: 152158. https://doi.org/10.1016/j.apsusc.2021.152158

[43] Akbayrak S, Özkar S. Ruthenium(0) NPs Supported on Multiwalled Carbon Nanotube As Highly Active Catalyst for Hydrogen Generation from Ammonia Borane. ACS Applied Materials & Interfaces 2012; 4: 6302-6310. https://doi.org/10.1021/am3019146

[44] Sun T, Wang Y, Long Y, Li Q, Fan G. Ultrafast, dry microwave-assisted surface property modulations to boost carbon stabilized Ru nanocatalyst for catalytic hydrogen evolution. Fuel 2022; 309: 122203. https://doi.org/10.1016/j.fuel.2021.122203

[45] Akbayrak S, Özcifci Z, Tabak A. Noble metal NPs supported on activated carbon: Highly recyclable catalysts in hydrogen generation from the hydrolysis of ammonia borane. Journal of Colloid and Interface Science 2019; 546: 324-332. https://doi.org/10.1016/j.jcis.2019.03.070

[46] Chu H, Li N, Qiu X, Wang Y, Qiu S et al. Poly(N-vinyl-2-pyrrolidone)-stabilized ruthenium supported on bamboo leaf-derived porous carbon for NH3BH3 hydrolysis. International Journal of Hydrogen Energy 2019; 44: 29255-29262. https://doi.org/10.1016/j.ijhydene.2019.01.248

[47] Liang H, Chen G, Desinan S, Rosei R, Rosei F et al. In situ facile synthesis of nanocluster catalyst supported on carbon black for hydrogen generation from the hydrolysis of ammonia borane. International Journal of Hydrogen Energy 2012; 37: 17921-17927. https://doi.org/10.1016/j.ijhydene.2012.09.026

[48] Du C, Ao Q, Cao N, Yang L, Luo W et al. Facile synthesis of monodisperse ruthenium NPs supported on graphene for hydrogen generation from hydrolysis of ammonia borane. International Journal of Hydrogen Energy 2015; 40: 6180-6187. http://dx.doi.org/10.1016/j.ijhydene.2015.03.070

[49] Cao N, Luo W, Cheng G. One-step synthesis of graphene supported Ru NPs as efficient catalysts for hydrolytic dehydrogenation of ammonia borane. International Journal of Hydrogen Energy 2013; 38: 11964-11972. https://doi.org/10.1016/j.ijhydene.2013.06.125

[50] Fu L, Cai L. Ru NPs loaded on tannin immobilized collagen fibers for catalytic hydrolysis of ammonia borane. International Journal of Hydrogen Energy 2021; 46: 10749-10762. https://doi.org/10.1016/j.ijhydene.2020.12.152

[51] Lv H, Wei R, Guo X, Sun L, Liu B. Synergistic catalysis of binary RuP nanoclusters on nitrogen-functionalized hollow mesoporous carbon in hydrogen production from the hydrolysis of ammonia borane. Journal of Physical Chemistry Letters 2021; 12: 696-703. https://doi.org/10.1021/acs.jpclett.0c03547

[52] Zhang L, Wang Y, Li J, Ren X, Lv H et al. Ultrasmall Ru Nanoclusters on Nitrogen-Enriched Hierarchically Porous Carbon Support as Remarkably Active Catalysts for Hydrolysis of Ammonia Borane. ChemCatChem 2018; 10: 4924-4930. https://doi.org/:10.1002/cctc.201801192

[53] Wei L, Yang Y, Yu YN, Wang X, Liu H et al. Visible-light-enhanced catalytic hydrolysis of ammonia borane using RuP2 quantum dots supported by graphitic carbon nitride. International Journal of Hydrogen Energy 2021; 46: 3811-3820. https://doi.org/:10.1016/j.ijhydene.2020.10.177

[54] Cheng W, Zhao X, LuoW, Zhang Y, Wang Y et al. Bagasse-derived carbon-supported ruthenium NPs as catalyst for efficient dehydrogenation of ammonia borane. ChemNanoMat 2020; 6: 1251-1259. https://doi.org/10.1002/cnma.202000215

[55] Akbayrak S, Özcifci Z, Tabak A. Activated carbon derived from tea waste: A promising supporting material for metal NPs used as catalysts in hydrolysis of ammonia borane. Biomass and Bioenergy 2020; 138: 105589. https://doi.org/10.1016/j.biombioe.2020.105589

[56] Song H, Cheng Y, Li B, Fan Y, Liu B et al. Carbon Dots and $RuP_2$ Nanohybrid as an Efficient Bifunctional Catalyst for Electrochemical Hydrogen Evolution Reaction and Hydrolysis of Ammonia Borane. ACS Sustainable Chemistry & Engineering 2020; 8: 3995-4002. https://doi.org/10.1021/acssuschemeng.0c00745

[57] Song Q, Wang WD, Hu X, Dong Z. Ru nanoclusters confined in porous organic cages for catalytic hydrolysis of ammonia borane and tandem hydrogenation reaction. Nanoscale 2019; 11: 21513-21521. https://doi.org/10.1039/c9nr08483e

[58] Liu Y, Yong X, Liu Z, Chen Z, Kang Z et al. Unified Catalyst for Efficient and Stable Hydrogen Production by Both the Electrolysis of Water and the Hydrolysis of ammonia borane. Advanced Sustainable Systems 2019; 3: 1800161. https://doi.org/10.1002/adsu.201800161

[59] Lu R, Xu C, Wang Q, Wang Y, Zhang Y et al. Ruthenium nanoclusters distributed on phosphorus-doped carbon derived from hypercrosslinked polymer networks for highly efficient hydrolysis of ammonia borane. International Journal of Hydrogen Energy 2018; 43: 18253-18260. https://doi.org/10.1016/j.ijhydene.2018.08.070

[60] Fan G, Liu Q, Tang D, Li X, Bi J et al. Nanodiamond supported Ru NPs as an effective catalyst for hydrogen evolution from hydrolysis of ammonia borane. International Journal of Hydrogen Energy 2016; 41: 1542-1549. https://doi.org/10.1016/j.ijhydene.2015.10.083

[61] Fernandes R, Patel N, Edla R, Bazzanella N, Kothari DC et al. Ruthenium NPs supported over carbon thin film catalyst synthesized by pulsed laser deposition for hydrogen production from ammonia borane. Applied Catalysis, A: General 2015; 495: 23-29. https://doi.org/10.1016/j.apcata.2015.01.034

[62] Fan Y, Li X, He X, Zeng C, Fan G et al. Effective hydrolysis of ammonia borane catalyzed by ruthenium NPs immobilized on graphitic carbon nitride. International Journal of Hydrogen Energy 2014; 39: 19982-19989. https://doi.org/10.1016/j.ijhydene.2014.10.012

[63] Akbayrak S, Cakmak G, Özturk T, Özkar S. Rhodium(0), Ruthenium(0) and Palladium(0) NPs supported on carbon-coated iron: Magnetically isolable and reusable catalysts for hydrolytic dehydrogenation of ammonia borane. International Journal of Hydrogen Energy 2021; 46: 13548-13560. https://doi.org/10.1016/j.ijhydene.2020.02.023

[64] Umegaki T, Ohta M, Xu Q, Kojima Y. Effect of salt addition on morphology and activity of in situ synthesized silica-ruthenium-nickel hollow sphere catalyst for hydrolysis of ammonia borane. Journal of Sol-Gel Science and Technology 2022; 104: 97-104. https://doi.org/10.1007/s10971-022-05925-7

[65] Yao Q, Shi W, Feng G, Lu ZH, Zhang X et al. Ultrafine Ru NPs embedded in $SiO_2$ nanospheres: Highly efficient catalysts for hydrolytic dehydrogenation of ammonia borane. Journal of Power Sources 2014; 257: 293-299. https://doi.org/10.1016/j.jpowsour.2014.01.122

[66] Akbayrak S, Kaya M, Volkan M, Özkar S. Ruthenium(0) NPs supported on magnetic silica coated cobalt ferrite: Reusable catalyst in hydrogen generation from the hydrolysis of ammonia borane. Journal of Molecular Catalysis A: Chemical 2014; 394: 253-261. https://doi.org/10.1016/j.molcata.2014.07.010

[67] Zhang X, Zhang Q, Peng Y, Ma X, Fan G. Oxygen vacancies and morphology engineered $Co_3O_4$ anchored Ru NPs as efficient catalysts for ammonia borane hydrolysis. International Journal of Hydrogen Energy 2022; 47: 7793-7801. https://doi.org/10.1016/j.ijhydene.2021.12.122

[68] Prabu S, Vinu M, Chiang KY. Ultrafine Ru NPs in shape control hollow octahedron MOF derived cobalt oxide@carbon as high efficiency catalysts for hydrolysis of ammonia borane. Journal of the Taiwan Institute of Chemical Engineers 2022; 139: 104511. https://doi.org/10.1016/j.jtice.2022.104511

[69] Cai J, Ding J, Wei D, Xie X, Li B et al. Coupling of Ru and O-vacancy on 2D Mo-based electrocatalyst via a solid-phase interface reaction strategy for hydrogen evolution reaction. Advanced Energy Materials 2021; 11: 2100141. https://doi.org/10.1002/aenm.202100141

[70] Badding CK, Soucy TL, Mondschein JS, Schaak RE. Metal ruthenate perovskites as heterogeneous catalysts for the hydrolysis of ammonia borane. ACS Omega 2018; 3: 3501-3506. https://doi.org/10.1021/acsomega.7b02003

[71] Ozgur DO, Simsek T, Ozkan G, Akkus MS, Ozkan G. The hydroloysis of ammonia borane by using amberlyst-15 supported catalysts for hydrogen generation. International Journal of Hydrogen Energy 2018; 43: 10765-10772. https://doi.org/10.1016/j.ijhydene.2018.01.037

[72] Zhang M, Liu L, He T, Li Z, Wu G et al. Microporous crystalline γ-$Al_2O_3$ replicated from microporous covalent triazine framework and its application as support for catalytic hydrolysis of ammonia borane. Chemistry - An Asian Journal 2017; 12: 470-475. https://doi.org/10.1002/asia.201601631

[73] Rachiero GP, Demirci UB, Miele P. Facile synthesis by polyol method of a ruthenium catalyst supported on γ-Al2O3 for hydrolytic dehydrogenation of ammonia borane. Catalysis Today 2011; 170: 85-92. https://doi.org/10.1016/j.cattod.2011.01.040

[74] Ma Y, Li X, Zhang Y, Chen L, Wu J et al. Ruthenium NPs supported on $TiO_2$(B) nanotubes: Effective catalysts in hydrogen evolution from the hydrolysis of ammonia borane. Journal of Alloys and Compounds 2017; 708: 270–277. https://doi.org/10.1016/j.jallcom.2017.02.239

[75] Konus N, Karatas Y, Gulcan M. In Situ Formed Ruthenium(0) NPs supported on $TiO_2$ catalyzed hydrogen generation from aqueous solution of ammonia borane at room temperature under air. Synthesis and Reactivity in Inorganic, Metal-Organic, and Nano-Metal Chemistry 2016; 46: 534-542. https://doi.org/10.1080/15533174.2014.988808

[76] Akbayrak S, Tanyıldızı S, Morkan İ, Özkar S. Ruthenium(0) NPs supported on nanotitania as highly active and reusable catalyst in hydrogen generation from the hydrolysis of ammonia borane. International Journal of Hydrogen Energy 2014; 39: 9628-9637. https://doi.org/10.1016/j.ijhydene.2014.04.091

[77] Tonbul Y, Akbayrak S, Özkar S. Nanozirconia supported ruthenium(0) NPs: Highly active and reusable catalyst in hydrolytic dehydrogenation of ammonia borane. Journal of Colloid and Interface Science 2018; 513: 287–294. https://doi.org/10.1016/j.jcis.2017.11.037.

[78] Kalkan EB, Akbayrak S, Özkar S. Ruthenium(0) NPs supported on nanohafnia: A highly active and long-lived catalyst in hydrolytic dehydrogenation of ammonia borane. Molecular Catalysis 2017; 430: 29–35. https://doi.org/10.1016/j.molcata.2016.11.0424

[79] Akbayrak S, Tonbul Y, Özkar S. Ceria-supported ruthenium NPs as highly active and long-lived catalysts in hydrogen generation from the hydrolysis of ammonia borane. Dalton Trans 2016; 45: 10969–10978. https://doi.org/10.1039/C6DT01117A

[80] Akbayrak S, Özkar S. Ruthenium(0) NPs supported on xonotlite nanowire: a long-lived catalyst for hydrolytic dehydrogenation of ammonia borane. Dalton Transactions 2014; 43: 1797-1805. https://doi.org/10.1039/C3DT52701H

[81] Song Y, Zhang T, Bai R, Zhou Y, Li L et al. Catalytically active Rh species stabilized by zirconium and hafnium on zeolites. Inorganic Chemistry Frontiers 2022; 9: 2395-2402. https://doi.org/10.1039/d2qi00280a

[82] Wang N, Sun Q, Zhang T, Mayoral A, Li L et al. Impregnating Subnanometer Metallic Nanocatalysts into Self-Pillared Zeolite Nanosheets. Journal of the American Chemical Society 2021; 143: 6905-6914. https://doi.org/10.1021/jacs.1c00578

[83] Deka JR, Saikia D, Hsia KS, Kao HM, Yang YC et al. Ru NPs embedded in cubic mesoporous silica SBA-1 as highly efficient catalysts for hydrogen generation from ammonia borane. Catalysts 2020; 10: 267. https://doi.org/10.3390/catal10030267

[84] Yao Q, Lu ZH, Yang K, Chen X, Zhu M. Ruthenium NPs confined in SBA-15 as highly efficient catalyst for hydrolytic dehydrogenation of ammonia borane and hydrazine borane. Scientific Reports 2015; 5: 15186. https://doi.org/10.1038/srep15186

[85] Chen M, Zhou L, Di L, Yue L, Ning H et al. RuCo bimetallic alloy NPs immobilized on multi-porous MIL-53(Al) as a highly efficient catalyst for the hydrolytic reaction of ammonia borane. International Journal of Hydrogen Energy 2018; 43: 1439-1450. https://doi.org/10.1016/j.ijhydene.2017.11.160

[86] Yang K, Zhou L, Yu G, Xiong X, Ye M et al. Ru NPs supported on MIL-53(Cr, Al) as efficient catalysts for hydrogen generation from hydrolysis of ammonia borane. International Journal of Hydrogen Energy 2016; 41: 6300-6309. https://doi.org/10.1016/j.ijhydene.2016.02.104

[87] Liu T, Wang Q, Yan B, Zhao M, Li W et al. Ru NPs supported on MIL-101 by double solvents method as high-performance catalysts for catalytic hydrolysis of ammonia borane. Journal of Nanomaterials 2015; 679526. https://doi.org/10.1155/2015/679526

[88] Wen L, Su J, Wu X, Cai P, Luo W et al. Ruthenium supported on MIL-96: An efficient catalyst for hydrolytic dehydrogenation of ammonia borane for chemical hydrogen storage. International Journal of Hydrogen Energy 2014; 39: 17129-1755. https://doi.org/10.1016/j.ijhydene.2014.07.179

[89] Cao N, Liu T, Su J, Wu X, Luo W et al. Ruthenium supported on MIL-101 as an efficient catalyst for hydrogen generation from hydrolysis of amine boranes. New Journal of Chemistry 2014; 38: 4032-4035. https://doi.org/10.1039/C4NJ00739E

[90] Wen L, Zheng Z, Luo W, Cai P, Cheng G. Ruthenium deposited on MCM-41 as efficient catalyst for hydrolytic dehydrogenation of ammonia borane and methylamine borane. Chinese Chemical Letters 2015; 26: 1345-1350. https://doi.org/10.1016/j.cclet.2015.06.019

[91] Akbayrak S. Decomposition of formic acid using tungsten(VI) oxide supported AgPd NPs. Journal of Colloids and Interface Sciences 2019; 538: 682-688. https://doi.org/10.1016/j.jcis.2018.12.074

[92] Yan Z, Xie J, Fang Y, Chen M, Wei X et al. $WO_3$ NPs Synthesized Through Ion Exchange Route as Pt Electrocatalyst Support for Alcohol Oxidation. Fuel Cells 2014; 14: 291-295. https://doi.org/10.1002/fuce.201200133

[93] Li F, Gong H, Wang Y, Zhang H, Wang Y et al. Enhanced activity, durability and anti-poisoning property of Pt/$W_{18}O_{49}$ for methanol oxidation with a sub-stoichiometric tungsten oxide $W_{18}O_{49}$ support. Journal of Material Chemistry A 2014; 2: 20154-20163. https://doi.org/10.1039/c4ta04220d

[94] Lu Y, Jiang Y, Gao X, Wang X, Chen W. Strongly coupled Pd nanotetrahedron/tungsten oxide nanosheet hybrids with enhanced catalytic activity and stability as oxygen reduction electrocatalysts Journal of American Chemical Society 2014; 136: 11687–11697. https://doi.org/10.1021/ja5041094

[95] Xi Z, Erdosy D, Mendoza-Garcia A, Duchesne P, Li J et al. Pd NPs Coupled to $WO_{2.72}$ Nanorods for Enhanced Electrochemical Oxidation of Formic Acid Nano Letters 2017; 17: 2727–2731. https://doi.org/10.1021/acs.nanolett.7b00870

[96] Li X, Yan Y, Jiang Y, Wu X, Li S et al. Ultra-small Rh NPs supported on WO3−x nanowires as efficient catalysts for visible-light-enhanced hydrogen evolution from ammonia borane. Nanoscale Advances 2019; 1: 3941-3947. https://doi.org/10.1039/C9NA00424F

[97] Lou Y, He J, Liu G, Qi S, Cheng L et al. Efficient hydrogen evolution from the hydrolysis of ammonia borane using bilateral-like $WO_{3-x}$ nanorods coupled with $Ni_2P$ NPs. Chemistry Communications 2018; 54: 6188-6191. https://doi.org/10.1039/C8CC03502D

[98] Chen W, Fu W, Qian G, Zhang B, Chen D et al. Synergistic Pt-$WO_3$ Dual Active Sites to Boost Hydrogen Production from Ammonia Borane. iScience. 2020; 23: 100922. https://doi.org/10.1016/j.isci.2020.100922

[99] Akbayrak S, Tonbul Y, Özkar S. Tungsten(VI) oxide supported rhodium NPs: Highly active catalysts in hydrogen generation from ammonia borane. International Journal of Hydrogen Energy 2021; 46: 14259-14269. https://doi.org/10.1016/j.ijhydene.2021.01.156

[100] Park KC, Jang IY, Wongwiriyapan W, Morimoto S, Kim YJ et al. Carbon-supported Pt–Ru NPs prepared in glyoxylate-reduction system promoting precursor–support interaction. Journal of Material Chemistry A 2010; 20: 5345–5354. https://doi.org/10.1039/B923153F

[101] Bock C, Paquet C, Couillard M, Botton GA, MacDougall BR. Size-Selected Synthesis of PtRu Nano-Catalysts: Reaction and Size Control Mechanism. Journal of American Chemical Society 2004; 126: 8028–8037. https://doi.org/10.1021/ja0495819

[102] Zhang X, Chan KY. Water-in-oil microemulsion synthesis of platinum-ruthenium NPs, their characterization and electrocatalytic properties. Chemistry of Materials 2003; 15: 451-459. https://doi.org/10.1021/cm0203868

[103] Kerkhof FPJM, Moulijn JA, Heeres A. The XPS spectra of the metathesis catalyst tungsten oxide on silica gel. Journal of Electron Spectroscopy and Related Phenomena. 1978; 14: 453-466. http://doi.org/10.1016/0368-2048(78)87004-2

[104] Khyzhun OY, Solonin YM, Dobrovolsky VD. Electronic structure of hexagonal tungsten trioxide: XPS, XES, and XAS studies. Journal of Alloys and Compounds 2001; 320: 1–6. http://doi.org/10.1016/S0925-8388(00)01454-7

[105] Akbayrak S, Özkar S. Inverse relation between the catalytic activity and catalyst concentration for the ruthenium(0) NPs supported on xonotlite nanowire in hydrogen generation from the hydrolysis of sodium borohydride. Journal of Molecular Catalysis A Chemical 2016; 424: 254–260. http://doi.org/10.1016/j.molcata.2016.09.001

[106] Manna J, Akbayrak S, Özkar S. Nickel(0) NPs supported on bare or coated cobalt ferrite as highly active, magnetically isolable and reusable catalyst for hydrolytic dehydrogenation of ammonia borane, Journal of Colloid and Interface Science 2017; 508; 359–368. http://doi.org/10.1016/j.jcis.2017.08.045

[107] Chu H, Li N, Qiu S, Zou Y, Xiang C et al. Ruthenium supported on nitrogen-doped porous carbon for catalytic hydrogen generation from $NH_3BH_3$ hydrolysis. International Journal of Hydrogen Energy 2019; 44: 1774–1781. http://doi.org/10.1016/j.ijhydene.2018.11.101

[108] Basu S, Brockman A, Gagare P, Zheng Y, Ramachandran PV et al. Chemical kinetics of Ru-catalyzed ammonia borane hydrolysis, Journal of Power Sources 2009; 188: 238–243. https://doi.org/10.1016/j.jpowsour.2008.11.085

[109] Zhou Q, Yang H, Xu C. Nanoporous Ru as highly efficient catalyst for hydrolysis of ammonia borane. International Journal of Hydrogen Energy 2016; 41: 12714-12721. https://doi.org/10.1016/j.ijhydene.2016.05.128

[110] Taşçı E, Akbayrak S, Özkar S. Ruthenium(0) NPs supported on silica coated $Fe_3O_4$ as magnetically separable catalysts for hydrolytic dehydrogenation of ammonia borane. International Journal of Hydrogen Energy 2018; 43: 15124-15134. http://doi.org/10.1016/j.ijhydene.2018.06.058

[111] Mori K, Miyawaki K, Yamashita H. Ru and Ru–Ni NPs on TiO2 Support as Extremely Active Catalysts for Hydrogen Production from Ammonia–Borane. ACS Catalysis 2016; 6: 3128-3135. https://doi.org/10.1021/acscatal.6b00715

[112] Roy S, Pachfule P, Xu Q. High catalytic performance of MIL-101-immobilized NiRu alloy NPs towards the hydrolytic dehydrogenation of ammonia borane. European Journal of Inorganic Chemistry 2016; 27: 4353–4357. https://doi.org/10.1002/ejic.201600180

[113] Akbayrak S, Erdek P, Özkar S. Hydroxyapatite supported ruthenium(0) NPs catalyst in hydrolytic dehydrogenation of ammonia borane: Insight to the NPs formation and hydrogen evolution kinetics. Applied Catalysis B: Environmental 2013; 142–143: 187–195. http://doi.org/10.1016/j.apcatb.2013.05.015

[114] Zahmakiran M. Preparation and characterization of LTA-type zeolite framework dispersed ruthenium NPs and their catalytic application in the hydrolytic dehydrogenation of ammonia-borane for efficient hydrogen generation. Materials Science and Engineering B 2012; 177: 606–613. https://doi.org/10.1016/j.mseb.2012.03.003

**Supplementary Material**

**Materials**

Ammonia borane ($NH_3BH_3$, 97%), ruthenium(III) chloride hydrate ($RuCl_3 \cdot 3H_2O$, 99.0%), tungsten(VI) oxide ($WO_3$, 98%, average particle size of 100 nm, surface area of 9.7 $m^2/g$) and sodium borohydride ($NaBH_4$, 98%) were purchased from Sigma-Aldrich. Deionized water was distilled by water purification system (Milli-Q System). All glassware and Teflon-coated magnetic stir bars were cleaned with acetone, followed by copious rinsing with distilled water before drying in an oven at 150 °C.

**Instrumentation**

Ruthenium content of $Ru/WO_3$ samples was determined by the Inductively Coupled Plasma Optical Emission Spectroscopy (ICP-OES, Leeman-Direct Reading Echelle) after each sample was completely dissolved in the mixture of $HNO_3$/HCl (1/3 ratio). Transmission electron microscopy (TEM) was performed on a JEM-2100F (JEOL) microscope operating at 200 kV. Samples were examined at magnification between 400 K and 700 K. The X-ray photoelectron spectroscopy (XPS) analysis was performed on a Physical Electronics 5800 spectrometer equipped with a hemispherical analyzer and using monochromatic Al Kα radiation of 1486.6 eV, the X-ray tube working at 15 kV, 350 W and pass energy of 23.5 keV. The binding energy scale was referenced to the C1s signal of 284.5 eV. Powder X-ray diffraction (XRD) patterns were acquired on a Rigaku Mini Flex X-ray diffractometer (radiation source Cu Kα, λ = 0.15418 nm, and scanning rate = 2 $min^{-1}$). Field emission scanning electron microscopy (FE-SEM) and energy dispersive spectroscopy (EDS) were performed by using a ZEISS GeminiSEM 500.

**Catalytic activity of $Ru/WO_3$ in hydrolysis of AB**

The hydrolysis reaction was performed in a jacketed reaction flask (20 mL) containing the $Ru^0/WO_3$ catalyst. The temperature of the reaction was adjusted by circulating water through the jacket of the flask from a constant temperature bath. A graduated glass tube filled with water was connected to the flask to measure the volume of the $H_2$ gas generated during the hydrolysis reaction. Next, 1.0 mmol of AB, $NH_3BH_3$, (31.8 mg) was added into the flask and the reaction medium was stirred at 1000 rpm. The volume of $H_2$ gas was measured by recording the displacement of water level every 1.0 min at constant atmospheric pressure.

**Turnover frequency (TOF) calculation**

Turnover frequency was calculated as described elsewhere [100] by the following equation:

$$\mathrm{TOF} = \frac{n(\mathrm{H_2})}{n(\mathrm{Ru}) \times \mathrm{t}}$$

where TOF is the turnover frequency in $min^{-1}$, $n(H_2)$ is the mole number of collected $H_2$ in mmol, n(Ru) is the mole number of total ruthenium in $Ru^0/WO_3$ in mmol, t is the time elapsed for the 40% conversion of ammonia borane. Note that TOF value was not corrected for the fraction of active sites.